Available online at www.sciencedirect.com

ScienceDirect

MATTER AND RADIATION AT EXTREMES

Matter and Radiation at Extremes 3 (2018) 300–311

www.journals.elsevier.com/matter-and-radiation-at-extremes

Research Article

Intensities and shifts of Lyman and Balmer lines of hydrogen-like ions in high density plasmas

G.P. Zhao [a], L. Liu [a,*], J.G. Wang [a], R.K. Janev [b], J. Yan [a]

[a] *Institute of Applied Physics and Computational Mathematics, P. O. Box 8009-26, Beijing 100088, China*
[b] *Macedonian Academy of Sciences and Arts, P. O. Box 428, 1000 Skopje, Macedonia*

Received 16 March 2018; revised 28 June 2018; accepted 4 July 2018
Available online 27 September 2018

Abstract

The spectral line intensities and line shifts of Lyman and Balmer series for transitions up to $n = 5$ of hydrogen-like ion are studied in plasmas with densities and temperatures in the ranges $n_e \sim 10^{18}$–10^{21} cm^{-3}, $T_e = 0.3$–1.2 eV respectively. The screened potential used to describe the interaction between charged particles includes the electron exchange-correlation and finite-temperature gradient effects and is valid for both weakly and strongly coupled plasmas. The dependencies of alpha, beta and gamma line shifts of Lyman and Balmer series on plasma density (for fixed temperature) and temperature (for fixed density) are investigated. The results for the H_α line shifts are compared with the available high-density experimental data.

PACS codes: 32.70.Jz; 32.70.-n; 52.27.Gr

Keywords: Screened coulomb interaction; Hydrogen-like ion; Spectral lines; High density plasmas

1. Introduction

The radiation emitted from a plasma is the main source of information about its composition, basic physical parameters (density and temperature), dynamical processes occurring in the plasma, and the interactions between its constituents [1–3]. As a collection of interacting charged particles (electrons and ions), the plasma is characterized by the ratio of the average potential to kinetic energy (Coulomb coupling parameter) $\Gamma = \frac{e^2/\overline{a}}{k_B T_e}$ where $\overline{a} = (3/4\pi n_e)^{1/3}$ is the average inter-electron distance, k_B is the Boltzmann constant and n_e and T_e are the plasma density and temperature, respectively. Plasmas with $\Gamma \ll 1$ and $\Gamma \gg 1$ are classified as weakly and strongly coupled plasmas, respectively. Another parameter that characterizes the plasma is its electron degeneracy $\theta = T_e/T_F$, where $T_F = \hbar^2(3\pi^2 n_e)^{2/3}/2m_e$ is the Fermi temperature, $\hbar$ and m_e being the reduced Planck constant and electron mass, respectively. Plasmas with $\theta \ll 1$ and $\theta \gg 1$ are classified respectively as degenerate (quantum) and non-degenerate (classical) plasmas. The condition $\theta \ll 1$ implies that the electron de Broglie wavelength $\lambda_B = \hbar/(2m_e k_B T_e)^{1/2}$ is larger than $\overline{a}$.

Due to the many–body correlations of plasma particles, their mutual interaction is always screened and only when the condition $\lambda_D \gg \overline{a}$ is fulfilled, where $\lambda_D = (k_B T_e/4\pi e^2 n_e)^{1/2}$ is the plasma Debye length, the inter-particle interaction can be considered as Coulombic. The effective two-particle potential in plasmas is usually derived from the plasma dielectric response function in certain approximations. In the first order of the expansion of dielectric function over the electron wavenumber, the effective electron-ion potential has the Yukawa-type form

* Corresponding author.
E-mail address: liu_ling@iapcm.ac.cn (L. Liu).
Peer review under responsibility of Science and Technology Information Center, China Academy of Engineering Physics.

https://doi.org/10.1016/j.mre.2018.07.001

[4,5] $V(r) = Ze^2 \exp(-r/\lambda_s)$, where Z is the ion charge. For hot, dilute and weakly coupled plasmas, the scale length is $\lambda_s = \lambda_D$ (Debye-Hückel screening); while for dense and cold degenerate plasmas, it is given by $\lambda_s = \lambda_{TF} = 1/(4\pi e^2 \partial n_e/\partial\mu)$ (Thomas-Fermi screening), where μ is the plasma chemical potential. The inclusion of the next term in the expansion of dielectric response function leads to analytic expressions for the effective potential that, incorporating the finite-temperature gradient corrections to the free energy, exchange-correlation and other effects, describe the screening more completely [6–8]. These effects become particularly important in many high density laboratory and astrophysical plasmas, such as laser produced and inertial confinement plasmas, plasmas in semiconductor nanostructures (metal thin films, nanotubes, quantum wells and dots) [9] and in compact astronomical objects (white dwarfs, neutron stars) [10].

Quite recently a new analytic screened potential has been derived by Stanton and Murillo [11] using the orbital-free density functional theory which includes the quantum degeneracy, gradient corrections to the free energy, exchange-correlations and finite-temperature effects. The potential connects the limits of Debye-Hückel, Thomas-Fermi, Lindhard dielectric response function and Bohmian quantum hydrodynamics descriptions of the Coulomb interaction screening in both weakly and strongly coupled plasmas. The form of this potential is (atomic units will be used hereafter)

$$V(r) = \frac{Z}{2r}\left[(1+\alpha)e^{-r/\lambda_-} + (1-\alpha)e^{-r/\lambda_+}\right], \quad (1)$$

$$\lambda_\pm^2 = \frac{\nu\lambda_{TF}^2}{2b \pm 2\sqrt{b^2-\nu}}, \ \alpha = \frac{b}{\sqrt{b^2-\nu}}, \quad (2)$$

where $\lambda_{TF} = \{\pi\sqrt{2\beta}/[4\mathcal{I}_{-1/2}(\eta_0)]\}^{1/2}$ is the Thomas-Fermi screening length, accounting for the electron degeneracy, $\beta = 1/T_e$, and $\mathcal{I}_{-1/2}(\eta_0)$ is the Fermi-Dirac integral of order $-1/2$, defined as $\mathcal{I}_p(\eta) = \int_0^{+\infty} dx x^p (1+e^{x-\eta})$. The parameters ν and b account for the gradient correlations and exchange-correlation effects, respectively, and are defined as [11].

$$\nu = \sqrt{8\beta} I'_{-1/2}(\eta_0) \Big/ 3\pi, b = 1 - \gamma_0 \lambda_{TF}^{-2}, \quad (3)$$

$$\gamma_0 \approx \frac{1}{8}\beta\Theta[h(\Theta) - 2\Theta h'(\Theta)], \ \Theta = 2/\beta\left(3\pi^2 n_e\right)^{3/2}, \quad (4)$$

$$h(\Theta) = \frac{1 + 2.8343\Theta^2 - 0.2151\Theta^3 + 5.2759\Theta^4}{1 + 3.9431\Theta^2 + 7.9138\Theta^4}\tanh\left(\Theta^{-1}\right). \quad (5)$$

The parameter η_0 in the argument of the Fermi-Dirac function is related to the average plasma density n_e by the relation

$$n_e = \sqrt{2} I_{1/2}(\eta_0) \Big/ \left(\pi^2 \beta^{3/2}\right) \quad (6)$$

The potential (1) is valid only for $\nu < b^2$; in the opposite case, its exponential terms become oscillatory functions and the screening lengths $\lambda_\pm$ have somewhat different expressions [11]. It should be noted that for $b \to 1$ and $\nu \to 0$ $(\alpha \to 1)$, the potential (1) reduces to the Debye-Hückel potential [11]. It should be also noted that the parameters λ_- and λ_+ for a pair (n_e, T_e) of plasma parameter are not independent, but they are mutually related. The pair (λ_-, λ_+) corresponding to a plasma with parameters (n_e, T_e) will be abbreviated as $\lambda_\pm$ in the reminder of the paper.

It should be emphasized that the static screened potential (1), like those in Refs. [6,7] are derived in the long-wavelength limit of plasma dielectric response function. In general, the interactions among moving plasma particles are time dependent and can induce time- (or frequency-) dependent (dynamical) screening of the Coulomb interaction. The static approximation to the Coulomb interaction screening can be applied to atomic processes when their time-scale is much smaller than the time-scale of collective plasma modes (such as, e.g., oscillations) and for time-averaged plasma quantities [12]. We are not aware of any dynamic screened potential in analytic form. As the potential screening is determined by the imaginary part of the inverse dielectric response function (see Ref. [12]), which depends on both the electron wave number k and plasma frequency ω (accounting for the collective effects of plasma micro-fields), it is necessary to calculate the complete dielectric response function by the quantum-statistical methods and extract its imaginary part. The Green's function method proved to be the most appropriate one for this purpose, as discussed at the end of Sec.3.

The purpose of present work is to study the properties of spectral lines of Lyman and Balmer series of hydrogen-like ions in finite-temperature dense plasmas by using the screened potential (1). The calculations are performed for plasmas with densities and temperatures in the ranges $n_e \sim 10^{18}$–10^{21} cm^{-3}, $T_e = 0.3$–1.2 eV, typical for the atmospheres and outer layers of H- and He-rich white dwarfs [13]. Experimental spectroscopic studies of such plasmas are currently underway at the Sandia National Laboratory [14]. This parametric range spans both the weak and strong coupling plasma regimes.

The experimental and theoretical studies of the line radiation from plasmas have a long history. The theoretical and experimental methods for these studies are described in the books of Griem [1,15,16], Kunze [2] and Fujimoto [17], where references to the prior experimental and theoretical investigations in the field are also given. Most of the theoretical work has been done on the spectroscopy of hydrogen plasmas.

The paper is organized as follows. In Sec.2, we briefly outline our computational method. In Sec.3, we present and discuss the spectral line intensities and the density and temperature dependences of line shifts, we also give a comparison of calculated H_α line shifts with available experimental data. In Sec.4 we give our conclusions.

2. Theoretical method

The radial Schrödinger equation for a hydrogen-like ion with the potential (1) is

$$\left[-\frac{\mathrm{d}^2}{2\mathrm{d}r^2}+\frac{l(l+1)}{2r^2}+V(r;\ Z,\ \lambda_\pm)\right]P_{nl}(r;\ Z,\ \lambda_\pm)$$
$$=E_{nl}(Z,\ \lambda_\pm)P_{nl}(r;\ Z,\ \lambda_\pm). \tag{7}$$

Using the scaling transformations

$$\rho=Zr,\delta_\pm=Z\lambda_\pm,\varepsilon_{nl}(\delta_\pm)=E_{nl}(Z,\lambda_\pm)/Z^2 \tag{8}$$

Eq. (7) reduces to that for the hydrogen atom ($Z=1$)

$$\left[-\frac{\mathrm{d}^2}{2\mathrm{d}\rho^2}+\frac{l(l+1)}{2\rho^2}+V(\rho;\delta_\pm)\right]P_{nl}(\rho;\delta_\pm)=\varepsilon_{nl}(\delta_\pm)P_{nl}(\rho;\delta_\pm) \tag{9}$$

The transformations (8) lead to the Z-scaling of matrix elements

$$\langle P_{nl}(r;Z,\lambda_\pm)\big|r^k\big|P_{n'l'}(r;Z,\lambda_\pm)\rangle=Z^{-k}\langle P_{nl}(\rho;\delta_\pm)\big|\rho^k\big|P_{n'l'}(\rho;\delta_\pm)\rangle \tag{10}$$

The energies and wave functions of bound states in the potential (1) are determined by expanding the atomic states $\Psi_{nlm}(\boldsymbol{\rho};\ \delta_\pm)$ over an even tempered basis $\{\chi_{klm}(\boldsymbol{\rho};\ \delta_\pm)\}$ of Slater-type-orbital functions [18].

$$\Psi_{klm}(\boldsymbol{\rho};\delta_\pm)=\sum_k c_{nk}\chi_{klm}(\boldsymbol{\rho};\delta_\pm), \tag{11}$$

$$\chi_{klm}(\boldsymbol{\rho};\delta_\pm)=N_l[\xi_k(\delta_\pm)]\rho^l\mathrm{e}^{-\xi_k(\delta_\pm)}\rho Y_{lm}(\boldsymbol{\rho}), \tag{12}$$

$$\xi_k=\alpha\beta^k,k=1,2,...,N,$$

where $N_l[\xi_k(\delta_\pm)]$ is a normalization constant, $Y_{lm}(\boldsymbol{\rho})$ are the spherical harmonics, α and β are variational parameters and n, l and m are the usual quantum numbers. The coefficients c_{nk} in Eq. (11) are determined by diagonalization of atomic Hamiltonian which yields the scaled energies $\varepsilon_{nl}(\delta_\pm)$. The radial part, $R_{nl}(\rho;\delta_\pm)$, of the function $\Psi_{nlm}(\boldsymbol{\rho};\ \delta_\pm)$ is related to the function $P_{nl}(\rho;\delta_\pm)$ in Eq. (9) by $R_{nl}(\rho;\delta_\pm)=P_{nl}(\rho;\delta_\pm)/\rho$. The energy scaling in Eq. (8) is valid only in the non-relativistic approximation; for ions with nuclear charges above $Z\sim 10$, where instead of Eq. (7) the Dirac radial equation should be used, the Z-scaling of fine-structure energies is no more possible.

Besides of lifting the Coulomb degeneracy of angular momentum states, an important property of screened potential (1) (that at asymptotically large distances decreases faster than $-1/r^2$) can support only a finite number of bound states [19]. This implies that with the increasing screening, the energy E_{nl} of nl state decreases and at certain critical value of the screening it becomes zero. The potential (1) contains two screening lengths, λ_- and λ_+ (mutually related through the plasma temperature and density), and the nl state enters the continuum only for a combination of $\lambda^c_{-,nl}$ and $\lambda^c_{+,nl}$ corresponding to a $(n_\mathrm{e},\ T_\mathrm{e})$ pair of plasma parameters. The potential parameters $\lambda_\pm,\nu,b$ are related to the plasma parameters n_e, T_e through Eqs. (2), (3) and (6) in which the Fermi-Dirac integrals and their inversions (Eq. (6)) can be calculated by using accurate Padé approximants and rational function approximations available in Ref. [20] and Ref. [21], respectively.

Fig. 1 shows the lines of $(n_\mathrm{e},\ T_\mathrm{e})$ pairs for which the states 1*s*, 2*l*, 3*l*, 4*s*, 4*f*, 5*s* and 5*g* become unbound. The state is bound in the $(n_\mathrm{e},\ T_\mathrm{e})$ region above the corresponding line. In the same figure we show the $\Gamma=1$ line, separating the regions of weak and strong coupling plasma regimes. The black line in Fig. 1 represents the equation $\nu=b^2$; the region $\nu<b^2$ of validity of the potential (1) lies above this line.

Fig. 1 shows that in certain regions of the $(n_\mathrm{e},\ T_\mathrm{e})$ parametric space, some of the states are bound and others are not. This fact has obvious consequences on the plasma spectroscopic features (e.g. termination of spectral series at some upper levels).

The absorption oscillator strength for the $nl\to n'l'$ transition in hydrogen-like ions with nuclear charge Z is given by [22].

$$f_{nl,n'l'}(Z,\lambda_\pm)=f_{nl,n'l'}(\delta_\pm)=\frac{2\omega_{nl,n'l'}(\delta_\pm)}{3}\frac{l+1}{2l+1}|\langle P_{n'l'}|\rho|P_{nl}\rangle|^2. \tag{13}$$

where $\omega_{nl,n'l'}(\delta_\pm)=\varepsilon_{n'l'}(\delta_\pm)-\varepsilon_{nl}(\delta_\pm)$is the transition energy (frequency).

The radiative transition probability$A_{n'l',nl}(Z,\ \lambda_\pm)$for the$nl\to n'l'$ transition can be expressed in terms of that for hydrogen atom $A_{n'l',nl}(\delta_\pm)$ as (cf. Eq. (10))

$$A_{n'l',nl}(Z,\lambda_\pm)=Z^{-4}A_{n'l',nl}(\delta_\pm),$$
$$A_{n'l',nl}(\delta_\pm)=\frac{2(2l+1)}{2l'+1}\alpha^3\omega^2_{nl,n'l'}(\delta_\pm)f_{nl,n'l'}(\delta_\pm) \tag{14}$$

where α is the fine-structure constant. The oscillator strengths and radiative transition probabilities in hydrogen-like ions in finite-temperature quantum plasmas have been studied recently in detail [23] by using the screened potential (1).

Under local thermodynamic equilibrium conditions, the spectral line intensity associated with the transition $nl\to n'l'$ in

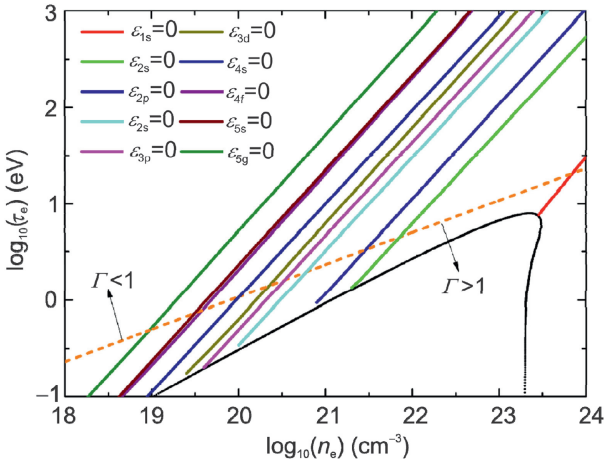

Fig. 1. The positions of critical screening lengths $\delta_\pm$ for 1s (red), 2s (green), 2p (blue), 3s (cyan), 3p (magenta), 3d (dark yellow), 4s (navy), 4f (purple), 5s (wine) and 5 g (olive) states in the (n_e, T_e) parametric space. The dashed line represents the Coulomb coupling parameter $\Gamma=1$ (orange). The region of validity of the potential (the condition$\nu<b^2$) lies above the black solid line$\nu=b^2$.

a hydrogen-like ion with charge Z embedded in a non-degenerate plasma is given by [24].

$$I_{n'l',nl}(Z,\lambda_{\pm}) = \Delta E_{n'l',nl}(Z,\lambda_{\pm})A_{n'l',nl}(Z,\lambda_{\pm})N_{n'l'}, \tag{15}$$

$$N_{n'l'} = N_{1s}(2l'+1)\exp(-\Delta E_{n'l',1s}/T_e), \tag{16}$$

where $N_{n'l'}$ and N_{1s} are the populations of the upper $|n'l'\rangle$ and the ground $|1s\rangle$ state, respectively, and T_e is the plasma temperature expressed in energy units. Keeping in mind the scaling relations (8) and (10) and introducing scaled temperature $\tau_e = T_e/Z^2$, we define the reduced scaled line intensity as

$$Z^2 I_{n'l',nl}(\delta_{\pm})/N_{1s} = (2l'+1)\omega_{n'l',nl}(\delta_{\pm})A_{n'l',nl}(\delta_{\pm})\exp(-\omega_{n'l',1s}/\tau_e). \tag{17}$$

The symbol $\delta_{\pm}$ in Eqs. (13–17) represents the combination of δ_- and δ_+ screening lengths corresponding to the values of $(n_e,\ T_e)$ pair for which the indicated quantities are calculated.

As mentioned in Sec.1 the energies $\varepsilon_{nl}(\delta_{\pm})$ decrease with the increasing screening and the transition frequency $\omega_{nl,n'l'}(\delta_{\pm}) = \varepsilon_{n'l'}(\delta_{\pm}) - \varepsilon_{nl}(\delta_{\pm})$ changes when the screening varies. In Ref. [23], it was shown that when the screening increases, the transition frequency associated with the $nl \rightarrow n'l'$ transition in the screened potential (1) is red-shifted (for $n \neq n'$) or blue-shifted (for $n = n'$) with respect to the pure Coulomb interaction (unscreened plasma) case. The n_e- and T_e-dependences of oscillator strengths and radiative transition probabilities (for fixed T_e and n_e, respectively) have also been studied in Ref. [23] for $nl \rightarrow n'l'$ Lyman and Balmer transitions with $n' \leq 5$.

As well known, the spectral lines in plasmas, besides by their intensity and frequency shift, are also characterized by their broadening, resulting from the thermal motion of emitting particle and its interaction with the surrounding plasma particles and plasma microfields. There is a vast amount of theoretical studies devoted to the spectral line shift and broadening in both dilute and dense plasmas (see, e.g. [15,16,25], respectively, and references therein). All the studies have been performed for hydrogen plasmas. While in the low-density limit the line shift and broadening can be described within the concept of an emitting atom embedded in an environment of perturbers, in dense plasmas their description has to include the many–body correlations, plasma degeneracy, dynamic interactions and collective plasma effects. An effective static screened potential of the form $(-Z/r)\xi(r)$, like the potential (1), by modifying the bound state binding energies and their differences, can provide information only about the line shift of spectral lines. The line broadening results from time-dependent processes in the plasma (e.g. collisions of the emitting atom/ion with plasma electrons and ions), plasma microfields effects (linear and quadratic Stark effects), multipole interactions and thermal (Doppler) effects [15,16,25–28]. The line broadening does not affect significantly the line intensity given by Eq. (17), but broadens its spectrum over a frequency range around the transition frequency $\omega_0 = \omega_{n'l',\ nl}$. The line intensity then takes the form

$$Z^2 I_{n'l',nl}(\delta_{\pm})/N_{1s} = (2l'+1)\omega_0 A_{n'l',nl}(\delta_{\pm})\exp(-\omega_{n'l',1s}/\tau_e)S(\omega), \tag{18}$$

where $S(\omega)$ is a profile function. The function $S(\omega)$ has a bell-shaped form (Lorentzian or Gaussian, or their combination), with its maximum at the transition frequency ω_0. Since the determination of $S(\omega)$ is outside the scope of the present work, for the purpose of representing uniformly the scaled reduced line intensities, we shall adopt a Lorentzian profile function, which is widely considered to be appropriate for dense plasmas [26–31].

$$F(\omega) = \frac{1}{\pi\Gamma}\left[\frac{\Gamma^2}{(\omega-\omega_0)^2+\Gamma^2}\right], \tag{19}$$

where Γ is the half-width at the half maximum (HWHM) of the line. In hydrogen plasmas with unscreened Coulomb electron-ion interaction, the main contribution to the line broadening is considered to be due to the linear Stark effect. If the electron-ion interaction is described by a static screened potential, the angular momentum degeneracy of the states with the same principle quantum number, as we have seen in Sec.2, is lifted by the short-ranged character of the potential (the finiteness of the screening length) and the linear Stark effect on the energy levels is absent. The plasma microfields can induce only second-order effects on the energies of nl-states (quadratic Stark effect). In order to represent the line intensities in a uniform way, we shall adopt the quasistatic expression for the HWHM from Ref. [32].

$$\Gamma = 2.16\frac{(n'^2-n^2)}{Z}F_0, \tag{20}$$

where n' and n are the principle quantum numbers of the upper and lower levels involved in the transition, and F_0 is the Holtsmark normal field strength

$$F_0 = 2\pi\left(\frac{4}{15}\right)^{2/3} n_e^{2/3}. \tag{21}$$

We should admit that the use of Eq. (20) for the half-width of $n'l' \rightarrow nl$ lines is obviously a rather crude approximation, except when the screening is small. However, as emphasized earlier, more accurate determination of the line width is outside the scope of the present work. We also note that the function (19) reduces the intensities calculated by Eq. (17) by a factor of $1/\pi\Gamma$.

In order to demonstrate the accuracy of the adopted line profile function, we present in Fig. 2 a comparison of calculated H_α line intensity in two plasmas, calculated by using the profile functions (19–21), with the experimental data from Ref. [29] (panel (a)) and Ref. [31] (panel (b)). The small peaks at the right wings of the experimental lines originate from the 667.8 nm He I line [29,31].

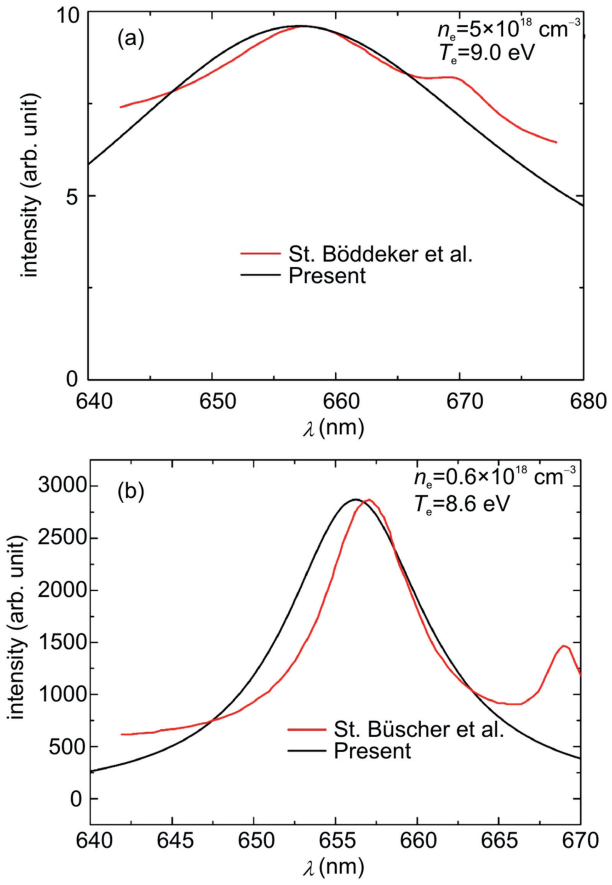

Fig. 2. Comparison of H_α line shapes calculated with Eqs. (19–21) for two plasmas with the experimental data of Ref. [29] (a) and Ref. [31] (b). The experimental peaks at 667.8 nm belong to He I line (cf. [29,31]).

3. Results and discussions

3.1. Dependences of line intensities on plasma temperature and density

We have performed line intensity calculations for the Lyman (np-1s) and the three branches (np-2s, nd-2p, ns-2p) of Balmer series transitions with $n \leq 5$ in the scaled temperature τ_e range 0.3–1.2 eV for three plasma densities: 10^{18}, 10^{19} and 10^{20}cm^{-3}. In the considered temperature range, the upper states involved in the above transitions are determined by the density (see Fig. 1): for $n_e = 10^{18}$cm^{-3} all states with $n \leq 5$ are bound and included in the calculations; for $n_e = 10^{19}$cm^{-3} the uppermost state is still bound in the potential depends on the value of τ_e (5p for $\tau_e = 0.3$ eV, 5d for $\tau_e = 0.4$ and 0.6 eV and 5 g for $\tau_e > 0.7$ eV), while for $n_e = 10^{20}$ cm^{-3} the line series terminate at 3s (for $\tau_e < 0.4$ eV), 3p (for $\tau_e = 0.6$ eV), 3d (for $\tau_e = 0.8$ eV), 4s (for $\tau_e = 1.0$ eV) and 4p (for $\tau_e = 1.2$ eV) upper states. The gradient correction effects and Coulomb coupling parameters, ν and Γ, are also quite different for these densities: for $n_e = 10^{18}$ cm^{-3}, $\nu \leq 0.05$, $\Gamma < 1$ for all τ_e values from the considered range, for $n_e = 10^{19}$ cm^{-3}, $\nu \leq 0.05$, $\Gamma > 1$ for $\tau_e < 0.5$ eV and $\Gamma < 1$ for $\tau_e > 0.5$ eV, and for $n_e = 10^{20}$ cm^{-3}, $\nu \leq 0.43$, $\Gamma > 1$ for all τ_e values from the considered range.

Below we show the results of our calculations for the lines of Lyman and Balmer series for the case of plasmas with density $n_e = 10^{19}$ cm^{-3} and a number of temperatures in the range 0.3–1.2 eV. The screening lengths $\delta_\pm$ of the potential, the gradient correction parameter ν, the Coulomb coupling parameter Γ and the states bound in the potential for these plasmas are shown in Table 1. For the plasmas with $\Gamma < 1$ we also show the values of Debye-Hückel screening lengths, which are very close to the values of δ_-. Table 1 indicates that $\Gamma \approx 1$ for $\delta_- \approx 32$ and $\delta_+ \approx 2.2$.

The scaled reduced line intensities of the Lyman and the three branches of the Balmer series transitions are shown in Figs. 3 and 4, respectively. We observe that line intensities increase with the increasing temperature. The increase of line intensity with τ_e for a given transition is related to the similar increase with τ_e of all the factors in Eq. (18) (exceptω_0, see [23]). It should also be noted that the lines are red-shifted and that the line shifts increase with decreasing the temperature.

In Figs. 5 and 6 we show the reduced scaled line intensities for the Lyman and Balmer series, respectively, for plasmas with a fixed scaled temperature $\tau_e = 0.4$ eV and a number of densities in the range $8 \times 10^{18} - 10^{20}$cm^{-3}. The gradient corrections parameters ν, the screening lengths $\delta_\pm$ of the potential and Coulomb coupling parameters Γ for these plasmas, as well as the bound states supported by the potential, are given in Table 2. As seen from the table all these plasmas are strongly coupled ($\Gamma > 1$).

Figs. 5 and 6 show that the peaks of line intensities decrease when density increases. This is in accord with the similar density dependence of radiative transition probabilities for $\Delta n \neq 0$ transitions [23]. With increasing plasma density the line shifts increase.

3.2. Dependences of line shifts on plasma temperature and density

As mentioned in the previous subsection, the variation of difference of bound state energies with varying the strength of the potential screening provides a possibility to investigate the dependence of line shifts on plasma density and temperature in a uniform way. The line shift dependence on density at high plasma densities has so far been investigated both theoretically [15,16,25–28] and experimentally [29–31] only for the H_α line within certain, relatively small temperature ranges, but the

Table 1
The strength ν of gradient corrections, Coulomb coupling parameter Γ, screening lengths $\delta_\pm$ and the bound states in the potential for plasmas with a mean electron density $n_e = 10^{19}$ cm^{-3} at a number of scaled temperatures τ_e (in eV units).

τ_e	ν	Γ	δ_-	δ_+	δ_D	Bound states
0.3	0.050 5	1.667 0	23.742 4	2.812 6		$n \leq 4$, 5s, 5p
0.4	0.028 5	1.250 2	27.721 2	2.410 4		$n \leq 4$, 5s, 5p, 5d
0.6	0.012 7	0.833 5	34.211 8	1.954 1	34.410 7	$n \leq 4$, 5s, 5p, 5d
0.8	0.007 2	0.625 1	39.607 2	1.688 3	39.734 1	$n \leq 5$
1.0	0.004 6	0.500 1	44.334 6	1.508 4	44.424 0	$n \leq 5$
1.2	0.003 2	0.416 7	48.596 9	1.376 2	48.664 1	$n \leq 5$

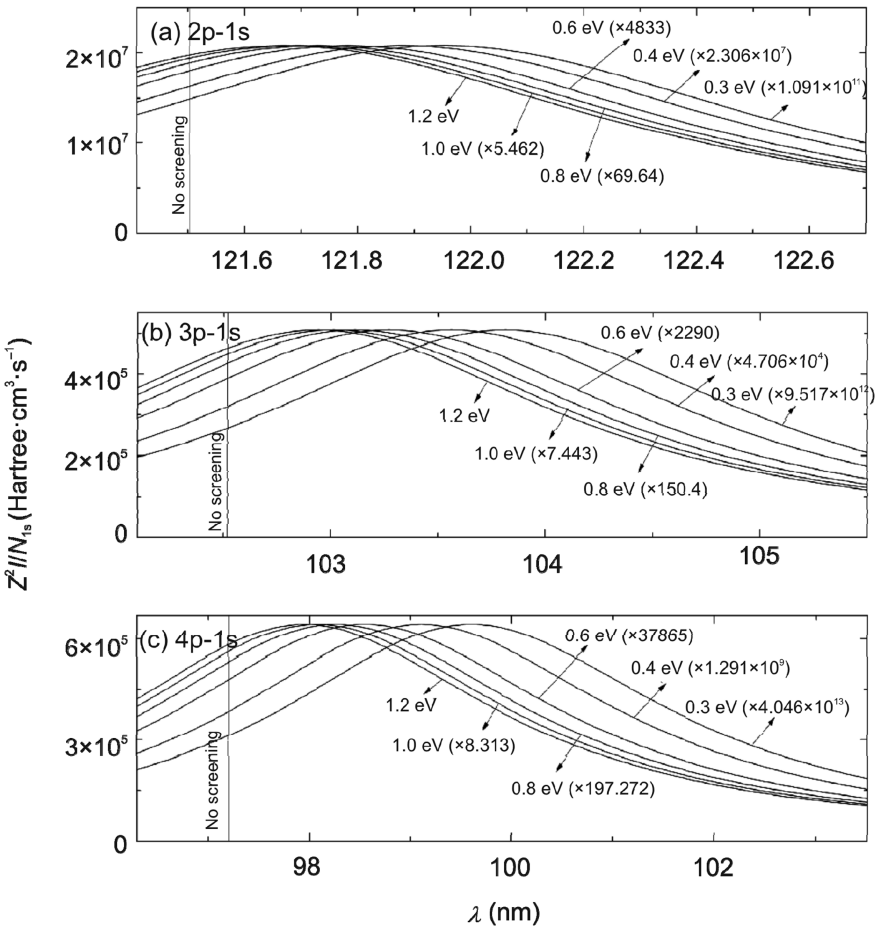

Fig. 3. Scaled reduced intensities of hydrogen-like ion Lyman lines in a plasma with mean electron density $n_e = 10^{19}$ cm^{-3} at different temperatures.

temperature dependence of the line shift, to the best of our knowledge, has never been investigated systematically.

In Figs. 7 and 8 we present the temperature dependences of Lyman-α, β, γ and Balmer-α, β, γ line shifts (the later calculated as 1/3 of the sum of *n*p-2s, *n*s-2p, *n*d-2p contributions, $n = 3, 4, 5$ for α, β, γ), respectively, in the temperature range 0.3–1.2 eV for the densities $n_e = 10^{18}$, 10^{19} and 10^{20}cm^{-3}. Fig. 7 shows that in the considered temperature range the line shift for Lyman-α, β, γ lines monotonically decreases with the increasing temperature for all selected plasma densities. This decrease results from the inverse proportionality of the wavelength with the transition frequency that increases with the increase of temperature (like in the case of Debye-Hückel and cos- Debye-Hückel potentials [33]). It should be noted that the line shift decrease is not linear. The figure shows that for the density $n_e = 10^{20}$ cm^{-3} the states 3p and 4p are unbound for $\tau_e < 0.6$ eV and $\tau_e < 1.2$ eV, respectively.

The temperature dependences of Balmer-α, β, γ line shifts, shown in Fig. 8, exhibit somewhat more complex behavior. For $n_e = 10^{18}$ cm^{-3} all three line shifts have a monotonic decrease with the increasing temperature in accord with the decrease of transition frequency with the increasing screening. The non-monotonic behavior of line shifts for 10^{19} cm^{-3} and 10^{20} cm^{-3} densities is a consequence of the fact that at certain temperatures one or both of the upper states contributing to the population of $n = 2$ manifold may be unbound for these densities. Thus, for $n_e = 10^{19}$ cm^{-3} the shift of Balmer-γ line at $\tau_e = 0.3$ eV is smaller than that for $\tau_e = 0.4$ eV because at $\tau_e = 0.3$ eV only the 5s-2p transition contributes to the population of $n = 2$ level and 5p and 5d states are unbound. The absence of Balmer-γ line shift for $n_e = 10^{20}$ cm^{-3} indicates that 5s, 5p and 5d states are all unbound in the considered temperature range (see Fig. 1). The figure also shows that for the same density and temperature the Balmer-α, β, γ line shifts are much larger than the corresponding Lyman line shifts. This is, of course, a reflection of the inverse proportionality of the wavelength with the transition frequency, which for the levels involved in the Balmer lines is much smaller than the one for the corresponding Lyman lines.

The density dependences of Lyman-α, β, γ and Balmer-α, β, γ line shifts in the interval $n_e = 8 \times 10^{18} - 8 \times 10^{20}$cm^{-3} for plasma temperatures $\tau_e = 0.4$ eV and $\tau_e = 1.0$ eV are shown in Figs. 9 and 10, respectively. We note that transition energy $\omega_{n'l',nl}$ $(n' > n)$, in an exponentially screened potential decreases with the increasing screening strength (through the increase of plasma density) [33]. Therefore the wavelength shift for the $nl \rightarrow n'l'$ transition should increase. Fig. 9

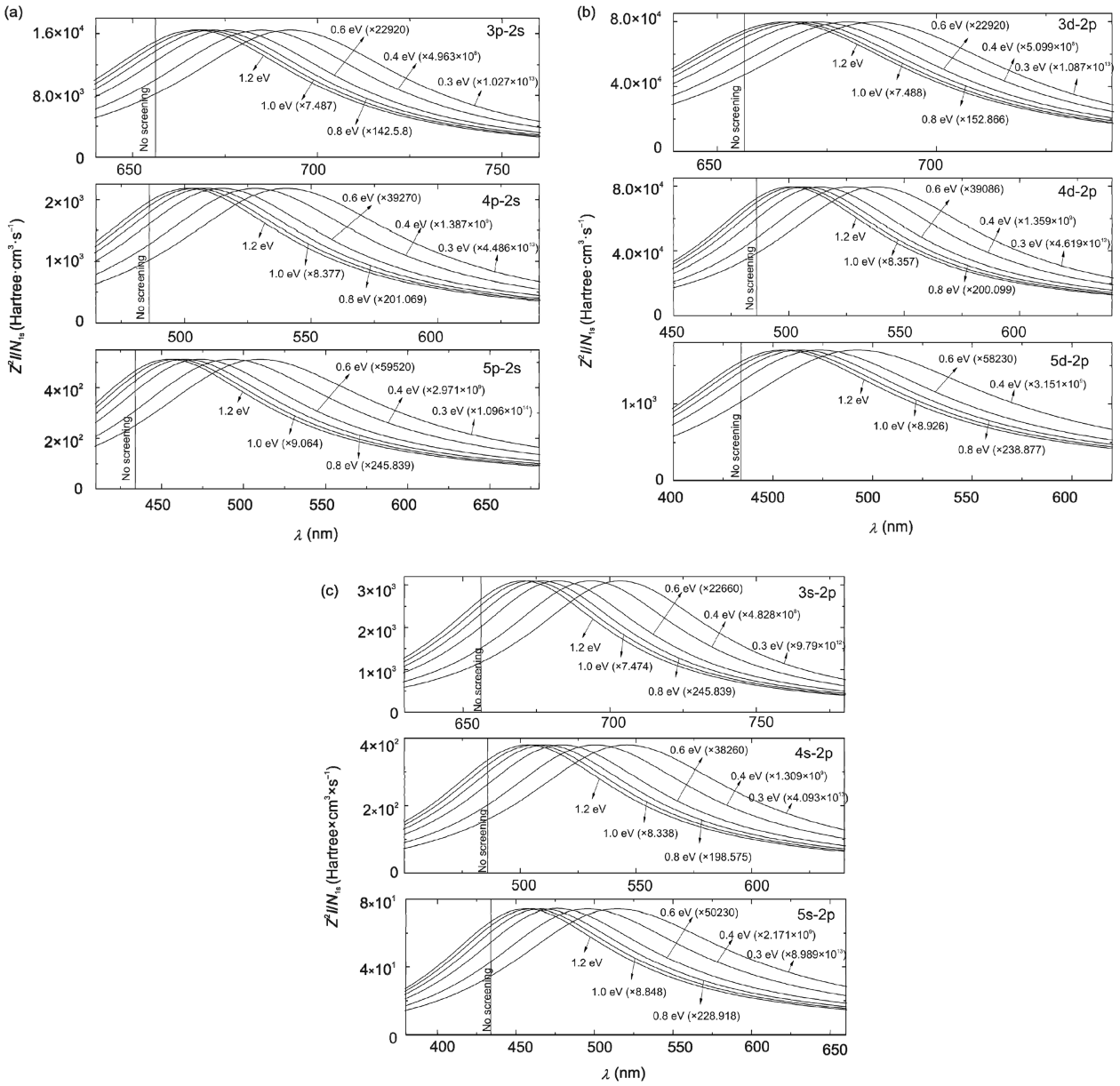

Fig. 4. Scaled reduced intensities of hydrogen-like ion Balmer *n*p-2s (a), *n*d-2p (b) and *n*s-2p (c) transitions in a plasma with mean electron density $n_e = 10^{19}$ cm^{-3} at different temperatures.

demonstrates this dependence for the shifts of Lyman-α, β, γ lines at both considered temperatures. As seen from the figure the line shift increase with density is non-linear.

In Fig. 10, the n_e-dependences of Balmer-α, β, γ line shifts are shown for 0.4 eV and 1.0 eV scaled temperatures. The monotonic non-linear increase of some of the line shifts with density turns into a decrease at certain densities at which some of the upper states of contributing transitions become unbound. For instance, to the Balmer-αline shift for $\tau_e = 0.4$ eV and $n_e = 8 \times 10^{19}$cm^{-3} contribute only the 3s-2p, 3p-2s transitions, while for $n_e = 10^{20}$ cm^{-3} at the same energy only the 3s-2p transition contributes. The Balmer-γ line shift n_e-dependence for $\tau_e = 0.4$ eV terminates at $n_e = 10^{19}$cm^{-3}, as 5s, 5p and 5d states are unbound for $n_e > 10^{19}$ cm^{-3} (see Fig. 1).

3.3. Comparison of balmer-α line shifts with experiments

As we mentioned earlier, most of the experimental studies of spectral line shifts and widths in dense plasmas have been performed for the hydrogen atom Balmer-α (H_α) line (see [29–31,34,35,37], and references therein) in rather limited ranges of plasma density and temperature. The focus of these investigations has been the density dependences of H_α line shift and width to test theoretical predictions. For the limited density ranges investigated usually a quasilinear density dependence of these quantities was observed (within the experimental uncertainties), in agreement with theoretical predictions [29–31]. Only a more careful analysis [28] of experimental data (by taking into account the temperature of

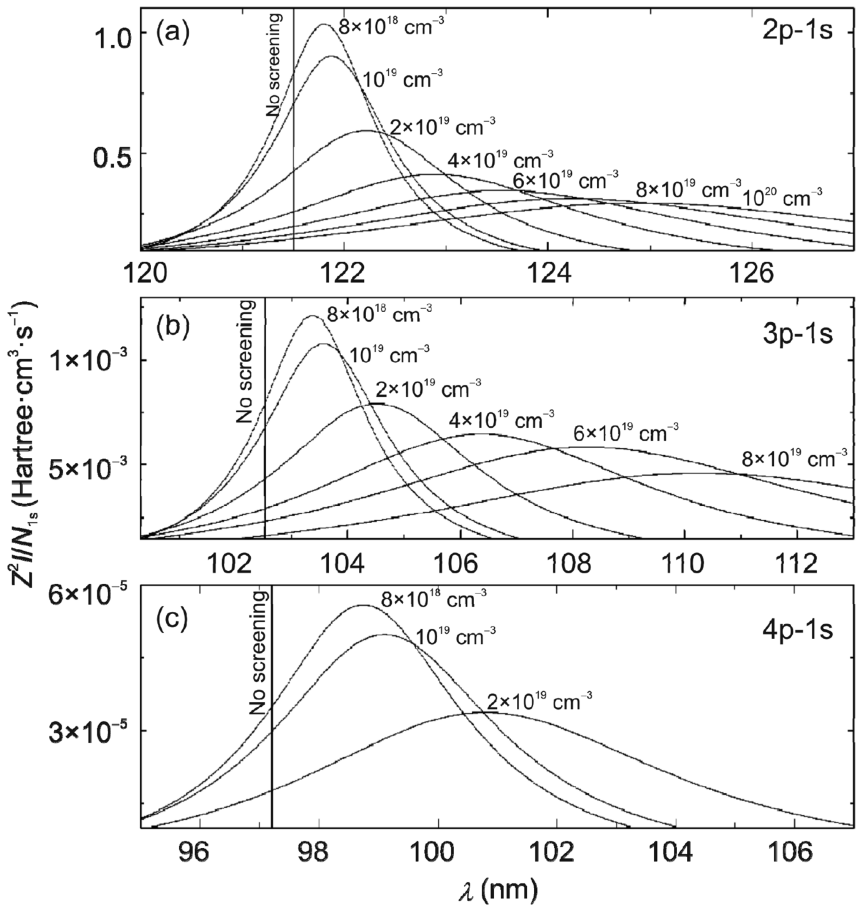

Fig. 5. Scaled reduced intensities of hydrogen-like ion Lyman lines in a plasma with temperature $\tau_e = 0.4$ eV and different densities.

their measurement) has shown that the experimental data of [29,31] in the combined density range $(0.45 - 10) \times 10^{18}\text{cm}^{-3}$ follow a non-linear density dependence, that agrees with both Griem's theory [36] (that includes dynamical contributions) and more sophisticated theoretical approaches [27,28] for the H_α line shift.

In Table 3 we compare the results of the present calculations for the H_α line shifts with experimental results of Ref. [29] for a number of plasma densities and temperatures in the ranges $(0.88 - 9.76) \times 10^{18}\text{cm}^{-3}$ and 5.6–10.2 eV. The results of theoretical calculations using the Griem's theory [36] and Green's function approach [25,26] (calculated in Ref. [29]) are also shown in the table and labelled as "Griem" and "Günter", respectively. In Table 3 we also give the values of Coulomb coupling parameter Γ and screening length λ_- for the considered plasmas, both indicating that these plasmas are weakly coupled ($\Gamma \ll 1$, $\delta_- \gg 32$). For comparison, we give in this table also the H_α line shifts calculated with the Debye-Hückel potential (the last column).

The results of the present calculations deviate from the experimental results by 22% on average. The Griem theory results have an average deviation from the experimental data of 23%, while the results of Green's function approach have a much smaller deviation (13%). The significant difference between the predictions of present, as well as Griem's theory, results and those of Green's function approach, can be attributed to the fact that the Green's function approach accounts for the dynamical effects in the screening much more completely than the Griem's theory, while the present calculations include only the static interaction effects.

In Table 4 we give a further comparison of the results of the present calculations with the experimental results of Ref. [31] in the density and temperature ranges $(0.49 - 2.54) \times 10^{18}\text{cm}^{-3}$ and 5.8–8.3 eV, respectively. The average deviation of present results from the experimental data is about 20%. It should be noted that the values of experimental densities and temperatures contain a significant level of uncertainty (especially in the temperature measurements where it is up to ±1.5 eV, see [31]).

Both theoretical and experimental results in Tables 3 and 4 show that the H_α line shift increases with the increasing density. In order to see the character of this increase we plot in Fig. 11 the experimental data and the results of present calculations, both taken from Tables 3 and 4, as function of density (The value of the shift at a given density relates to the corresponding temperature in Tables 3 and 4). The theoretical results of Ref. [28] (that include dynamical screening) are also shown. Their values at different densities also correspond to different temperatures. Fig. 11 shows that the density dependence of both experimental and theoretical results for H_α line

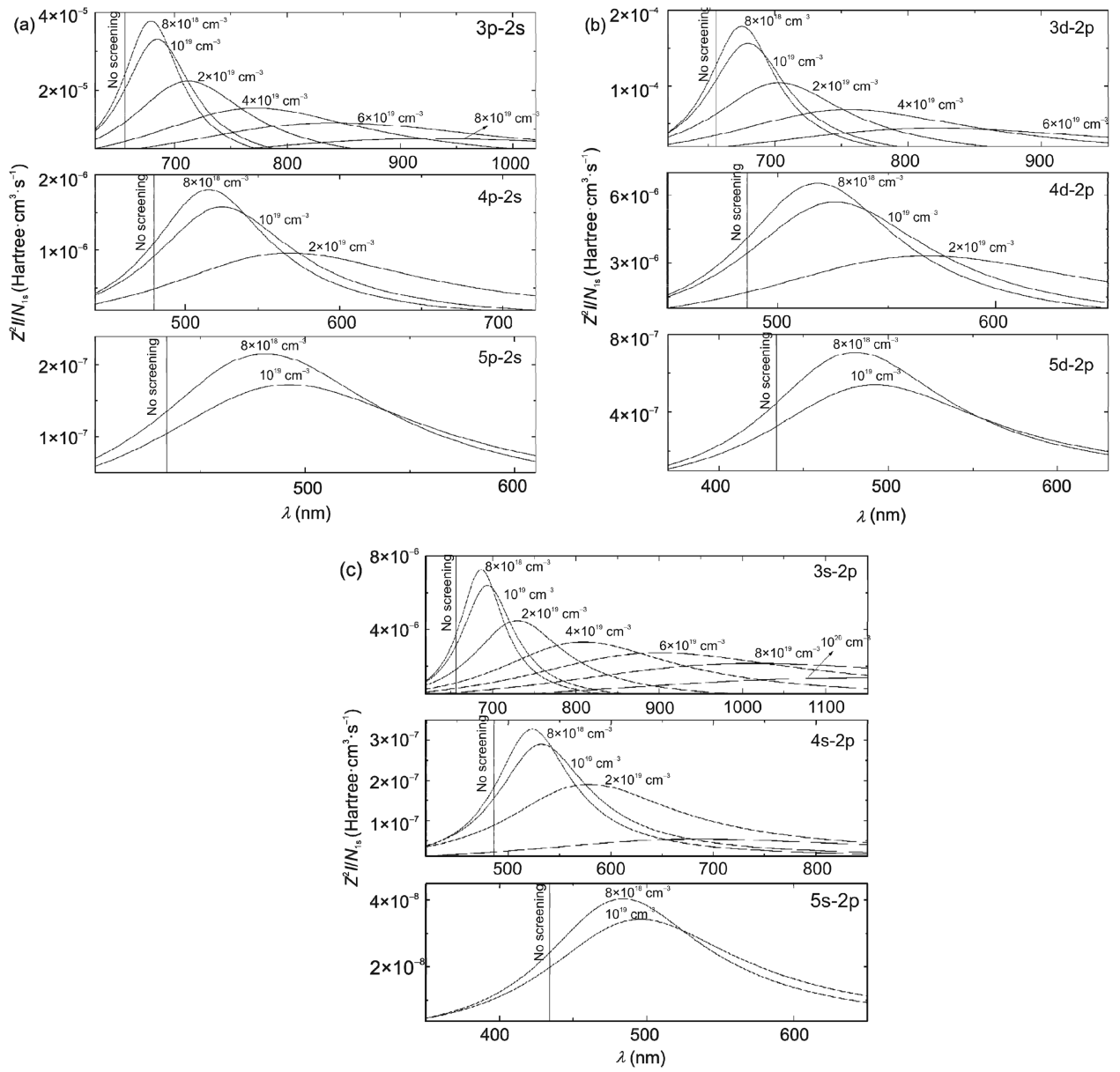

Fig. 6. Scaled reduced intensities of hydrogen-like ion Balmer np-2s (a), nd-2p (b) and ns-2p (c) transitions in a plasma with temperature $\tau_e = 0.4$ eV and different densities.

Table 2
The strength ν of gradient corrections, Coulomb coupling parameter Γ, screening lengths $\delta_\pm$ and the bound states supported by the potential for a plasma with scaled temperature $\tau_e = 0.4$ eV and a number of mean electron densities (in cm^{-3} units).

n_e	ν	Γ	δ_-	δ_+	Bound states
8×10^{18}	0.022 9	1.160 6	31.077 8	2.404 4	$n \leq 4$, 5s, 5p, 5d, 5f
10^{19}	0.028 5	1.250 2	27.721 2	2.410 4	$n \leq 4$, 5s, 5p, 5d
2×10^{19}	0.056 7	1.575 2	19.330 9	2.441 3	$n \leq 3$, 4s, 4p, 4d
4×10^{19}	0.111 8	1.984 6	13.271 2	2.508 8	$n \leq 3$, 4s
6×10^{19}	0.165 4	2.271 8	10.491 9	2.585 1	$n \leq 3$
8×10^{19}	0.217 5	2.500 4	8.766 9	2.673 2	$n \leq 2$, 3s, 3p
10^{20}	0.268 2	2.693 5	7.529 3	2.777 7	$n \leq 2$, 3s

shift in the considered density range is non-linear. This is in contrast with the linear density dependence of H_α line shift observed in plasmas with densities below 10^{18} cm^{-3} and temperatures below 1.6 eV (see [37], and references therein). The origin of non-linear increase of the line shift with density is the non-linear decrease of the energy difference between states involved in the transition when the density increases (or, equivalently, the decrease of the screening length $\lambda_-$with density increase; see Tables 3 and 4). This is a result of the fact that for a given temperature the energy of the upper states reaches its zero value at smaller densities (larger λ_-) than the lower one (see Fig. 1), implying a difference in the gradients of their energy decrease with the increasing density.

The validity of the present approach for calculation of line intensities and line shifts of spectral lines of hydrogen-like

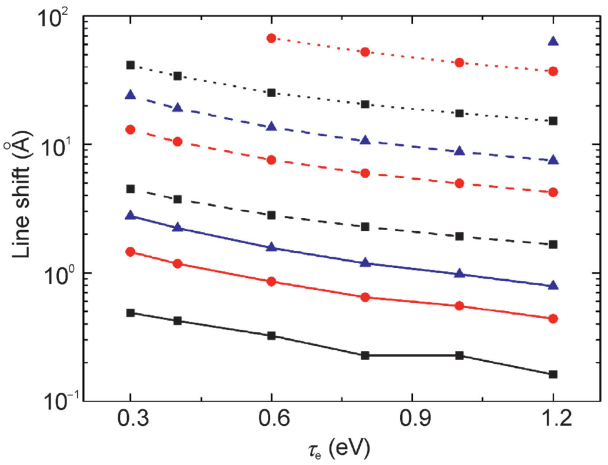

Fig. 7. Temperature dependence of line-shifts for Lyman-α (black), Lyman-β (red) and Lyman-γ (blue) lines for plasmas with mean electron densities $n_e = 10^{18}$ cm^{-3} (full lines), $n_e = 10^{19}$ cm^{-3} (dashed lines) and $n_e = 10^{20}$ cm^{-3} (dotted lines).

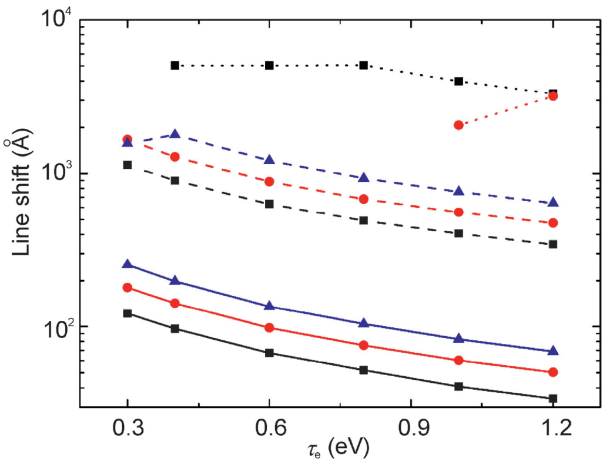

Fig. 8. Temperature dependence of Balmer-α (black), Balmer-β (red) and Balmer-γ (blue) line shifts for plasmas with mean electron densities $n_e = 10^{18}$ cm^{-3} (full lines), $n_e = 10^{19}$ cm^{-3} (dashed lines) and n_e=10^{20}cm^{-3} (dotted lines).

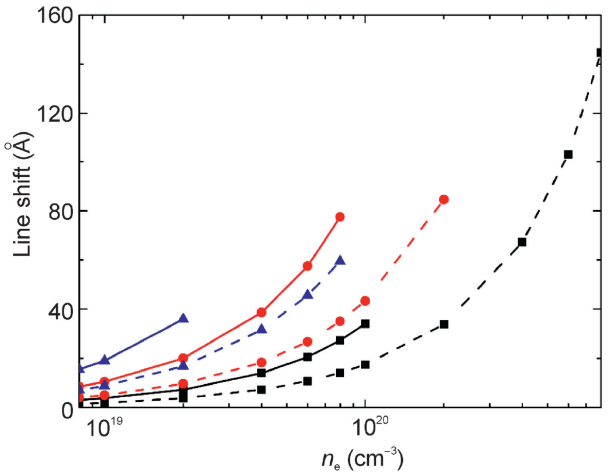

Fig. 9. Density dependence of Lyman-α (black), Lyman-β (red) and Lyman-γ (blue) line shifts in plasmas with temperatures $\tau_e = 0.4$ eV (full lines) and $\tau_e = 1.0$ eV (dashed lines).

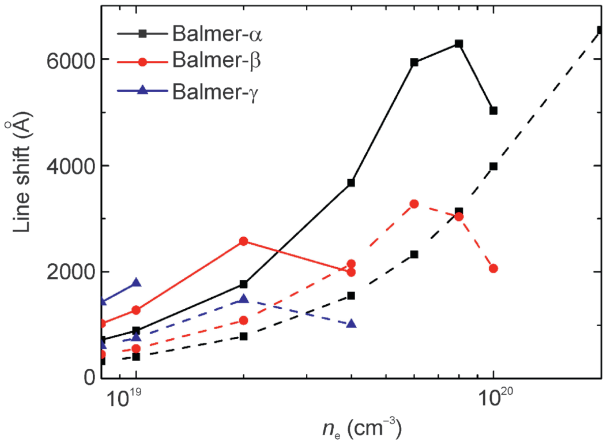

Fig. 10. Density dependence of Balmer-α (black), Balmer-β (red) and Balmer-γ (blue) line shifts for plasmas with plasma temperatures $\tau_e = 0.4$ eV (full lines) and $\tau_e = 1.0$ eV (dashed lines).

ions in plasmas relies on the validity of static potential (1) for description of the Coulomb interaction screening in the plasma. As mentioned in Sec.1 this potential accounts for the many–body correlations (beyond the pair-wise approximation of the many–body correlation function), quantum degeneracy, gradient corrections to the kinetic energy, electron exchange-correlations and finite-temperature plasma effects. In terms of plasma parameters its validity encompasses both low-*T*, high-density (quantum) plasmas and dilute-high temperature plasmas. By incorporating these effects, the static potential (1) can fairly accurately describe the atomic electron bound state energies in a plasma and thereby their variation with plasma parameters (and, consequently, the spectral line shifts). The standard approach for calculation of spectral line properties in dilute ($n_e < 10^{17}$ cm^{-3}) plasmas, based on the seminal papers of Griem and Baranger [38–40], uses a pure Coulomb interaction between the charged particles, but takes into account of effects of plasma micro-fields (linear and quadratic Stark effects) and electron-emitting atom collisions, and even the quadrupole interactions caused by the inhomogeneity of the local fields. These effects are responsible for the line shift and line broadening (and predict a linear red shift [37]). For high density plasmas ($n_e > 10^{18}$cm^{-3}), the many–body correlations have to be accounted by using the Green's function approach in which the self-energy, within the first order Born approximation for the electron-emitting atom collision, contains the imaginary part of the inverse dielectric response function [25,26] that includes the effects of time dependent micro-fields on the emitter (i.e. dynamical screening). Within this approach, the red line shift shows a non-linear density dependence [26]. A similar effect on the line shift is produced by taking into account the electron acceleration in the ion field when the plasma density is high [28] (as observed in Fig. 11).

Table 3
Comparison of experimental H_α line shifts of Ref. [29] with the present and other theoretical results.

$n_e(10^{18}cm^{-3})$	T_e (eV)	λ_-	$\Delta\lambda_{expt}$ (Å)	$\Delta\lambda_{Günter}$ (Å)	$\Delta\lambda_{Griem}$ (Å)	$\Delta\lambda_{present}$ (Å)	$\Delta\lambda_{Debye}$ (Å)
0.88	5.6	354.377 5	4.20 ± 0.38	4.69	6.07	5.670 410	5.672 363
1.00	5.7	335.390 4	5.33 ± 0. 30	5.35	6.79	6.617 188	7.561 035
1.30	6.0	301.798 4	6.73 ± 0. 72	7.00	8.50	8.508 301	9.453 125
1.39	6.1	294.286 5	7.25 ± 0.51	7.49	8.99	9.455 078	9.455 078
1.90	6.4	257.825 3	9.41 ± 1.20	10.27	11.82	12.291 50	12.292 48
2.34	7.0	242.970 4	11.24 ± 1.76	12.59	13.9	15.130 86	14.184 08
3.05	7.8	224.651 6	15.49 ± 3.22	16.16	17.11	17.971 19	16.077 15
4.00	8.5	204.781 8	19.66 ± 4.91	20.63	20.96	20.811 52	19.864 26
5.47	9.2	182.184 6	20.11 ± 5.58	26.99	26.84	27.441 89	25.547 85
6.88	9.8	167.660 2	22.99 ± 5.46	32.74	31.89	31.234 38	32.181 15
8.33	10.2	155.449 1	27.16 ± 6.88	38.76	36.78	35.975 59	35.975 10
9.76	10.4	145.011 3	35.43 ± 8.81	44.62	41.48	42.617 19	43.566 41

Table 4
Comparison of experimental H_α line shifts of Ref. [31] with the present calculations.

n_e ($10^{18}cm^{-3}$)	T_e (eV)	Γ	λ_-	$\Delta\lambda_{expt}$ (Å)	$\Delta\lambda_{present}$ (Å)	$\Delta\lambda_{Debye}$ (Å)
2.54	8.34	0.0380	254.553 6	17.6 ± 3.1	12.291 50	13.238 28
1.96	8.40	0.0346	290.820 7	12.3 ± 1.3	10.400 88	10.398 93
1.35	7.82	0.0328	338.104 1	9.7 ± 2.0	6.617 188	7.562 500
0.99	7.12	0.0325	376.735 5	4.8 ± 0.9	4.727 539	5.671 875
0.68	6.39	0.0319	430.635 9	2.8 ± 0.6	3.780 762	4.726 074
0.49	5.77	0.0317	482.063 5	2.6 ± 0.3	2.834 473	1.891 113

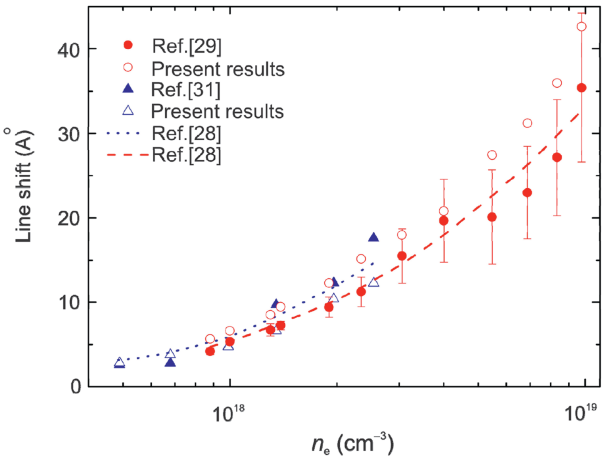

Fig. 11. Density dependence of H_α line shift. Closed symbols are experimental data from Ref. [29] (dots) and Ref. [31], open symbols are results of the present calculations, dashed and dotted lines are theoretical results of Ref. [28].

4. Conclusions

In the present work we have studied the intensities and shifts of Lyman and Balmer lines of hydrogen-like ions imbedded in warm high density plasmas. The effective charged particle interaction is described by a static potential (Eq. (1)) that includes the many–body correlations, electron degeneracy, gradient corrections to the free energy and exchange-correlation effects. The Schödinger equation for hydrogen-like ion with this potential is scalable with respect to nuclear charge. The eigenvalue problem was solved by using a large set of Slater-type-orbital basis functions. Intensities and line shifts of Lyman and Balmer transitions with upper states having principal quantum number $n \leq 5$ in the density and scaled temperature ranges $0.8 \times (10^{18}–10^{20})$ cm^{-3} and 0.3–1.2 eV, respectively, were calculated. As expected, the peaks of line intensities for a fixed plasma density increase with the increase of temperature, while for a fixed temperature they decrease with the increasing density. It is also shown that for a fixed density the shifts of Lyman- and Balmer-α, β, γ lines decrease with the increasing temperature, while for a fixed temperature they increase when density increases. In the case of Balmer line shifts, that represent an average of the line shifts of *n*p-2s, *n*s-2p, *n*d-2p transitions, the above density and temperature dependences can be violated at their upper side as one (or both) of *n*p and *n*d states can become unbound. The comparison of our results for the H_α line shift with experimental data in the density range $(0.5–10) \times 10^{18}cm^{-3}$ ($T_e = 5–10$ eV) shows on average an agreement within 20% and confirms the non-linear increase of the shift with density increase.

Conflict of interest

We declare that we do not have any commercial or associative interest that represents a conflict of interest in connection with the work submitted.

Acknowledgments

One of the co-authors (R. K. J.) is greatly indebted to Dr. E. Stambulchik for useful discussions on the line width in dense plasmas. This work was supported by the National Key Research and Development Program of China (Grant No. 2017YFA0402300), National Natural Science Foundation of China (Grants No. 11474033, 11474032 and 11534011) and Science Challenge Project (Grant No. TZ2016001).

References

[1] H.R. Griem, Plasma Spectroscopy, Mc Graw-Hill, New York, 1964.
[2] H.-J. Kunze, Introduction to Plasma Spectroscopy, Springer, Berlin, 2009.
[3] I.H. Hutchinson, Principles of Plasma Diagnostics, second ed., Cambridge Univ. Press, New York, 2009.

[4] D. Salzman, Atomic Processes in Hot Plasmas, Oxford Univ. Press, Oxford, 1998.
[5] M. Bonitz, Quantum Kinetic Theory, Teubner, Stuttgart/Leipzig, 1998.
[6] P.K. Shukla, B. Eliasson, Novel attractive force between ions in quantum plasmas, Phys.Rev. Lett. 108 (2012) 165007.
[7] M. Akbari-Moghanjoughi, Hydrodynamic limit of wigner-poisson kinetic theory: revisited, Phys. Plasmas 22 (2015) 022103.
[8] Z. Moldabekov, T. Schoof, P. Ludwig, M. Bonitz, Statically screened ion potential and Bohm potential in a quantum plasma, Phys. Plasmas 22 (2015) 102104.
[9] P. Harrison, A. Valavanis, Quantum Wells, Wires and Dots: Theoretical and Computational Physics of Semiconductor Nanostructures, fourth edition, Wiley, New York, 2016.
[10] S.L. Shapiro, S.A. Teukolski, Black Holes, White Dwarfs and Neutron Stars, Wiley, New York, 1983.
[11] L.G. Stanton, M.S. Murillo, Unified description of linear screening in dense plasmas, Phys. Rev. E 91 (2015) 033104.
[12] M.S. Murillo, J.C. Weiheit, Dense plasmas, screened interactions, and atomic ionization, Phys. Rep. 302 (1998) 1.
[13] P. Kowalski, The Physics of the Atmospheres of Cold White Dwarfs,, Ph.D. Dissertation, Vanderbilt Univ., 2006.
[14] M.H. Montgomery, R.E. Falcon, G.A. Rochau, J.E. Bailey, T.A. Gomez, et al., An experimental platform for creating white dwarf photospheres in the laboratory: preliminary results, High. Energy Density Phys. 17 (2015) 168.
[15] H.R. Griem, Spectral Line Broadening by Plasmas, Academic, New York, 1974.
[16] H.R. Griem, Principles of Plasma Spectroscopy, Cambridge Univ. Press, Cambridge, 1997.
[17] T. Fujimoto, Plasma Spectroscopy, Oxford Univ, Press, Oxford, 2004.
[18] J. Kuang, C.D. Lin, Convergent TCAO close-coupling calculations for electron transfer, excitation and ionization in intermediate keV He^{2+}-H collisions, J. Phys. B Atom. Mol. Opt. Phys. 30 (1997) 101.
[19] L.D. Landau, E.M. Lifshitz, Quantum Mechanics: Non-relativistic Theory, 1958. Pergamon, London.
[20] R.G. Dandrea, N.W. Ashcroft, A.E. Carlsson, Electron liquid at any degeneracy, Phys. Rev. B 34 (1986) 2097.
[21] H. Antia, Rational function approximations for Fermi-Dirac integrals, Astrophys. J. Suppl. 84 (1993) 101.
[22] H.A. Bethe, E.E. Salpeter, Quantum Mechanics of One- and Two-electron Atoms, Academic Press, New York, 1957.
[23] G.P. Zhao, L. Liu, J.G. Wang, R.K. Janev, Spectral properties of hydrogen-like ions in finite-temperature quantum plasmas, Phys. Plasmas 24 (2017) 053509.
[24] R.W. Cowan, The Theory of Atomic Structure and Spectra, Univ. of California Press, Berkeley, 1981.
[25] S. Günter, L. Hitzschke, G. Röpke, Hydrogen spectral lines with the inclusion of dense-plasma effects, Phys. Rev. 44 (1991) 6834.
[26] L. Hitzschke, G. Röpke, T. Seifert, R. Zimmermann, Green's function approach to the electron shift and broadening of spectral lines in non-ideal plasmas, J. Physiol. Biochem. 19 (1986) 2443.
[27] E. Oks, Advance in diagnostics for high-temperature plasmas based on the analytical result for the ion dynamical broadening of hydrogen spectral lines, Phys. Rev. E 60 (1999), R2480. A new spectroscopic effect resulting in a narrowing of hydrogen lines in dense plasmas, J. Quant. Spectrosc. Radiat. Transfer, 65 (2000) 405.
[28] E. Oks, Reduction of spectral line shifts due to the acceleration of electrons by the ion field in plasmas, J. Phys. B Atom. Mol. Opt. Phys. 35 (2002) 2251.
[29] St. Böddeker, S. Günter, A. Könies, L. Hitzschke, H.-J. Kunze, Shift and width of the H_α line of hydrogen in dense plasmas, Phys. Rev. E 47 (1993) 2785.
[30] S.A. Flih, E. Oks, Y. Vitel, Comparison of the Stark widths and shifts of the H-alpha line measured in a flash tube plasma with theoretical results, J. Phys. B Atom. Mol. Opt. Phys. 36 (2003) 283.
[31] S. Büscher, Th. Wrubel, S. Ferri, H.-J. Kunze, The Stark width and shift of the hydrogen H_α line, J. Phys. B Atom. Mol. Opt. Phys. 35 (2002) 2889.
[32] E. Stambulchik, Y. Maron, Stark effect of high-n hydrogen-like transitions: quasi-contiguous approximation, J. Phys. B Atom. Mol. Opt. Phys. 41 (2008) 095703. Quasicontiguous frequency-fluctuation model for calculation of hydrogen and hydrogenlike Stark-broadened line shapes in plasmas, Phys. Rev. E 87 (2013) 053108.
[33] Y.Y. Qi, J.G. Wang, R.K. Janev, Bound-bound transitions in hydrogenlike ions in Debye plasmas, Phys. Rev. A 78 (2008) 062511. Bound-bound transitions in hydrogen-like ions in dense quantum plasmas, Phys. Plasma 23 (2016) 073302.
[34] A. Escargual, E. Oks, J. Richau, D. Volodko, Highly nonlinear, sign-varying shift of hydrogen spectral lines in dense plasmas, Phys. Rev. E 62 (2000) 2667.
[35] A. Escarguel, B. Ferhat, A. Lesage, J. Richau, A single laser spark in aqueous medium, J. Quant. Spectrosc. Radiat. Transfer 64 (2000) 353.
[36] H.R. Griem, Shifts of hydrogen and ionized-helium lines from Δn=0 interactions with electrons in dense plasmas, Phys. Rev. 38 (1988) 2943.
[37] Y. Vitel, Experimental study of H_α broadening and shift in dense argon plasmas, J. Phys. B Atom. Mol. Phys. 20 (1987) 2327.
[38] H.R. Griem, A.C. Kolb, K.Y. Shen, Stark broadening of hydrogen lines in a plasma, Phys. Rev 116 (1959) 4. Stark Profile Calculations for the H_β Line of Hydrogen. Astrophys. J. 135 (1962) 272.
[39] M. Baranger, B. Moser, Light as a plasma probe, Phys. Rev. 123 (1961) 25.
[40] H.R. Griem, M. Baranger, A.C. Kolb, G.K. Oertel, Stark broadening of neutral helium lines in a plasma, Phys. Rev. 125 (1962) 177.